Substructure Energy Method for Prediction of Space Shuttle Modal Damping

Daniel D. Kana*
Southwest Research Institute, San Antonio, Texas
and
James F. Unruh†
Boeing Commercial Aircraft Company, Seattle, Wash.

The results of this program demonstrate the validity of a dissipative energy approach for predicting the damping of a four-component space shuttle model by means of modal parameters obtained from tests of the individual components. A relationship between modal damping energy per cycle and peak strain (or kinetic) energy is first determined empirically from test data for each component. Undamped analytical models of each component are also developed, and combined into a system model from which are obtained modal kinetic (or strain) energies for its respective modes. These data are then used with the empirical damping curves to apportion the proper amount of damping energy to each component in a combined system mode, and thereby allow a prediction of damping ratio. Some discrepancies in results are noted to occur because of incomplete modeling of connecting link mechanisms and anomalies in modal responses.

I. Introduction

THE complexity and size of the space shuttle vehicle renders the task of full scale system dynamic testing extremely difficult. Nevertheless, system modal properties, including damping, must be acquired by some means for accurate prediction of dynamic response. It is also recognized that full scale testing of shuttle-type substructures is more feasible, and in fact, would be quite similar to previous testing of Saturn and other vehicles. Therefore, a technique has been sought for prediction of system properties from design parameters, as well as those measured on full scale tests of individual components. Currently-available analytical methods for synthesis of system mass and stiffness properties have been found to be entirely adequate for prediction of free natural modes.[1] However, synthesis of damping and development of techniques for its prediction have been found to be in a much less adequate state.

In previous work,[2] an energy approach was developed for correlating modal damping data which were obtained on components of a simple parallel stage shuttle model, and for further combination of those data into a prediction of modal damping for the combined system. Comparisons of predicted and measured data showed extremely good overall agreement for the relatively simple model. Therefore, it became appropriate to consider whether this energy approach was valid when applied to a more representative, four-component shuttle model. This paper presents the results of this further investigation, and is a condensation of more detailed information given in Ref. 3.

In conducting the investigation, our objectives can be summarized as follows:

1) Design a four-component, three-dimensional parallel stage shuttle model which includes liquids in the Hydrogen/Oxygen (H/O) tank, and which includes built-up construction and component connecting joints that simulate to some degree those envisioned for the base line shuttle design.

2) Develop an analytical model for the substructures and combine them into a model for the total system. Predict natural frequencies, modes, modal mass, modal stiffness and kinetic and strain energies from this model.

3) Perform dynamic tests of the substructures and joints to determine their properties. In particular, determine whether the previously derived damping energy correlation can be established for components of this design.

4) Use the previously developed energy method to predict the modal damping properties for the system.

5) Perform dynamic tests on the combined system to verify the adequacy of the analytical model and establish the applicability of the damping energy prediction method to this type of model.

Details of the analytical model development will not be presented herein, since they involved the use of already-known substructuring and eigenvalue techniques. However, it is useful for interpretation of the results to follow, to state that free-free rather than fixed-boundary component modes were used in the analysis.

Description of Physical Model

A drawing of the combined system model is shown in Fig. 1. The H/O component basically consists of two 0.005-in. wall stainless steel liquid propellant tanks, each having an ellipsoidal bulkhead, and joined together through an aluminum skirt section. The upper tank and skirt and the aluminum bulkheads have been used before in previous studies.[4] The lower tank is fabricated in two sections that are joined together with a ring flange. Ethylene glycol is used as a model propellant in both tanks. Ring and wire circumferential stiffeners are provided on both tanks to subdue localized shell mode response and thereby not obscure overall bending and longitudinal response.

Submitted April 8, 1974; presented at the AIAA/ASME/SAE 15th Structures, Structural Dynamics and Materials Conference, Las Vegas, Nevada, April 17-19, 1974; revision received December 12, 1974. The results presented herein were obtained under NASA Contract NAS 8-27569 for the Marshall Space Flight Center, Huntsville, Alabama. The authors wish to express their sincere appreciation to several people who aided in the conduct of this program. G.E. Ransleben performed most of the design of the mechanical apparatus; D.C. Scheidt, G.W. Downey, Jr., and F.S. Campbell performed the experiments. Special mention should also be given to R.W. Shock and J. Admire of the Marshall Space Flight Center, who as technical monitors, provided numerous useful suggestions that aided in the successful completion of this program.

Index category: Structural Dynamic Analysis.

*Manager, Structural Dynamics and Acoustics Section. Member AIAA.

†Specialist Engineer, Aircraft Noise Staff, Research Unit.

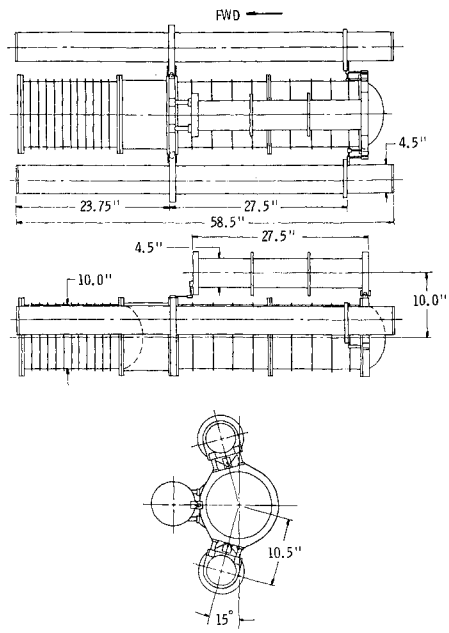

Fig. 1 General design of shuttle model.

The orbiter and two solid rocket motors (SRMs) are made of ¼-in. wall polyvinly chloride tubing. This material was chosen because it demonstrated modal damping of the order of 1% critical. It was felt that values in this range were desirable to allow reasonable measurement accuracy. Values from the all-metal H/O tank will be seen to be considerably lower. These components also were fitted with solid steel end and mounting rings to emphasize overall bending, longitudinal and torsional responses.

Mounting points for the several components were provided on a solid 1-in. thick steel disk and annular ring which formed part of the H/O tank. The disk forms the forward mounting point and attachment for a simulated free-free suspension, while the steel ring formed the aft mounting point. The forward orbiter and aft SRM joints consist of steel double flexures which are designed to be significantly stiff in the vertical dierection for each respective component, and very compliant (essentially only a guide) in the longitudinal direction. The aft orbiter and forward SRM joints consist of a three-dimensional pin arrangement. Further details of the design can be obtained from Ref. 3.

From the preceding description it can be seen that the combined model was designed to experience modes which include rigid body motion of the components against the mounting joints at low frequencies, various combinations of bending, torsion, and longitudinal response combined with spring motion at intermediate frequencies, and all three of the latter without significant spring motion at higher frequencies. The general range for frequencies of given types of modes was designed to be ratioed to corresponding modes for the baseline shuttle vehicle design, where possible. In this regard, however, liquid slosh modes were not brought into a range of significant coupling. Finally, it should be recognized that no external damping was applied to the system. Energy dissipation was confined to internal damping of the individual components and that of the six connecting links.

Experimental Procedures

A. Component Tests

The first series of component tests consisted of suspending each individual component on a low frequency suspension which approximated a free-free condition, and performing resonance tests. Mode shapes were qualitatively identified and frequencies noted. At the same time, measurements of damping and modal kinetic energy were measured. Damping was usually determined from free decay records. However, in some cases beating between closely spaced modes necessitated the use of the half-bandwidth technique, and in a few cases precluded any damping measurement at all. Measurement of modal kinetic energy was accomplished indirectly. Actually, dissipated energy per cycle at resonance was determined by measuring input force and displacement. The displacement at the point of maximum modal response on the structure was also measured. Damping energy per cycle C_c was then determined for a normalized maximum modal amplitude of one millimeter. Normalized modal kinetic energy T_o was then determined from $\bar{T}_o = \bar{D}_c/4\pi\zeta$, where ζ was determined by free decay. It should be noted that this procedure assumes the existence of damping linearity with response amplitude.

In carrying out this procedure, similar tests were run by excitation along three different perpendicular axes. On the orbiter and two SRMs it was found that modal properties, including damping, did not vary along the two transverse axes (i.e., the models were symmetrical). However, it was found that significant variations did occur in the H/O tank model. This apparently resulted because of the seam-welded tank construction, as well as the presence of some localized buckled areas in the lower tank. This problem was handled by postulating different models along the pitch and yaw axes of the H/O tank. These experiments were conducted only for nearly full liquid levels. In addition, measurements of pressure at the center of the two bulkheads aided in isolating longitudinal liquid modes. No measurements were made on lateral slosh modes.

B. Connecting Link Tests

Tests to determine damping properties of the connecting links were conducted on the links alone (i.e., not connected to the major components) before the major components were assembled. Double flexures were tested in pairs by means of a simulated mounting. The flexures were mounted on the H/O tank ring and this ring was clamped to a rigid mounting block. In place of the orbiter or SRM ring, the other ends of the flexures were joined on a solid steel bar. This bar had dimensions ¼-in. thick, 1-in. wide, and 5-in. long. Thus, the solid bar acted as a mass cantilevered on the two flexure pivots. This integral structure was resonance tested similar to the major components by excitation in each the vertical and side directions. Excitation in the longitudinal direction was not considered because of the inherent weakness in that direction. Damping ratios and kinetic energies were measured for several modes of this compound structure.

The 3-D pivot was also resonance tested in the vertical direction only. This was accomplished by mounting one side in the H/O ring, and mounting a solid block on the other end of the pivot. Only one mode could be identified in this manner. Testing in the side and longitudinal directions on this joint was not readily possible because of the large compliance in rotation along those axes.

C. System Tests

Procedures for system tests were essentially the same as for component testing. Modes and frequencies were qualitatively identified by observing the outputs of accelerometers mounted at various locations. The position of the exciter coil had to be changed several times in order to optimize the response of certain modes. Even so, a number of the modal responses were either too obscure, or beating instabilities between closely spaced modes prevented the acquisition of good data. Likewise, in some cases mixing of symmetric and antisymmetric modes occurred when they were closely spaced. On spite of these difficulties, a variety of numerous modes were identified and data obtained on them.

Free-Free Component Results

A. Major Components

Analytical modes and frequencies for the free-free com-

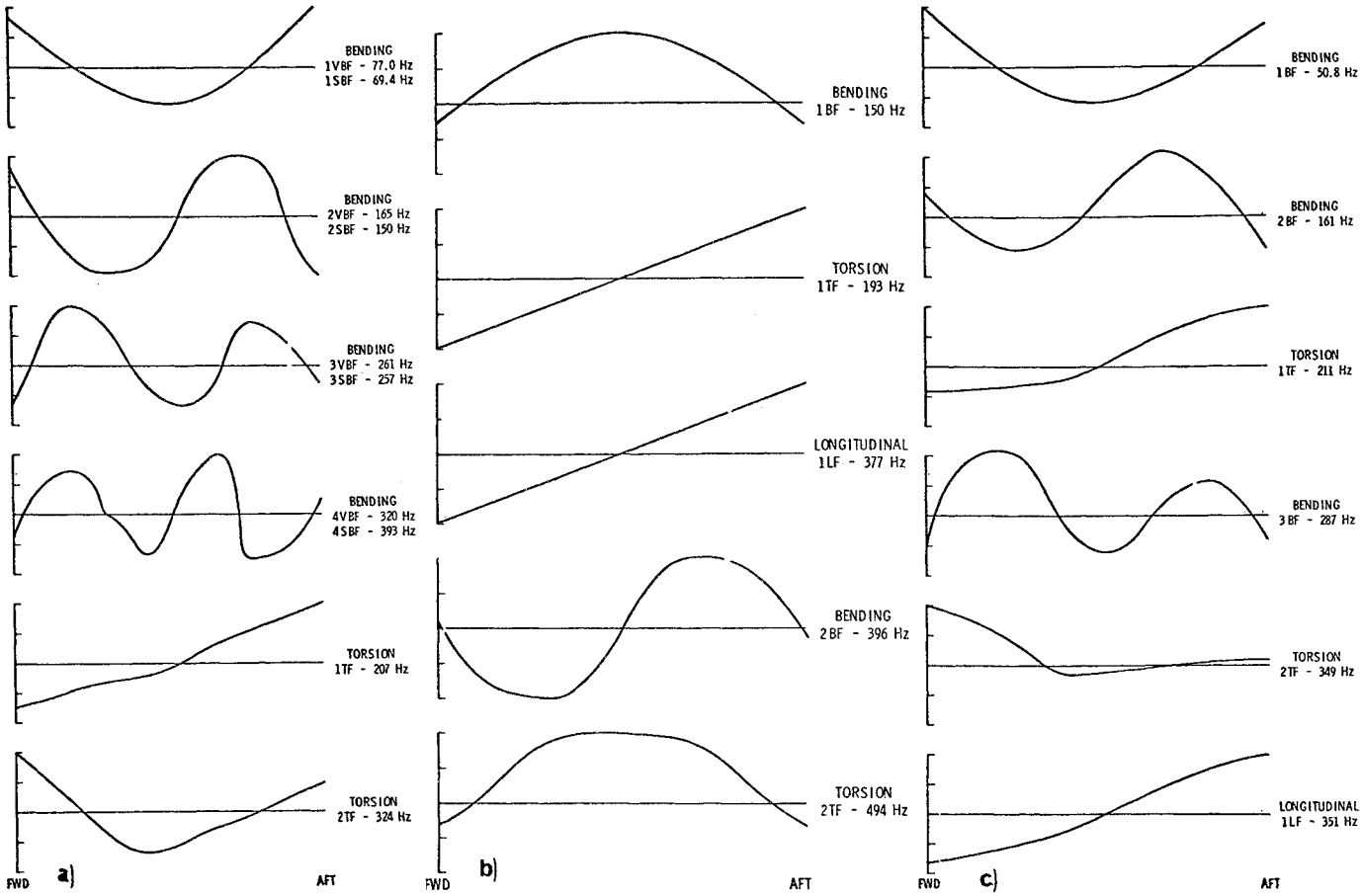

Fig. 2 Component modes for free-free suspension: a) H/O tank; b) orbiter; c) solid rocket motors.

ponents are presented in Fig. 2. Although more modes were determined , we show only those that are significant through a 400-Hz frequency range. The indicated mode identification abbreviations will be used from here on except that the (F), which indicates free test, will be dropped. Note that two frequencies are given for the bending modes of the H/O tank. This corresponds to the different stiffnesses that were experienced along orthogonal axes, as has been previously described.

A comparison of theoretical and experimental frequencies is given in Table 1. Measured damping data is also given for information. By appropriate adjustment of various analytical model stiffness parameters, it can be seen that excellent agreement was achieved in the frequencies. Although the experimental frequencies were essentially identical for the two SRMs, slight variations in damping can be noted.

Damping energy information for for H/O tank is presented in Fig. 3. It should be recognized that modal kinetic and strain energies are equal for such free-free resonances. It is obvious that basically two different damping processes occur, one associated with all types of modes of the structure itself, and one with the longitudinal modes of the liquid. It is not surprising that essentially two different mechanisms would influence damping processes for such modes. This formation of two different correlations was not encountered in the earlier work,[2] but can still be readily incorporated into the damping prediction method, as will be shown in the next section. It was gratifying to find that the damping energy data for the built-up component with liquid, did fall into some correlation pattern. This is an absolute requirement for the damping prediction method to be used.

Similar damping energy data are shown in Fig. 4 for the orbiter and two SRMs. Data for all types of modes correlate on the same line when normalized to the same amplitude. In this, torsional mode amplitudes were taken as that at the mean radius of the component tube wall. This is a new discovery that was not included in the earlier work because of a lack of different types of modes in that work. Although the orbiter geometry is significantly different from the SRMs, it still correlates on the same line. Since their material content is identical, it appears that the material alone that is strained during vibration is what influences the correlation line. Geometry differences and types of modes do not cause a separation in data. This in itself is an extremely important discovery for correlation of damping data from a design point of view.

B. Connecting Links

Damping energy data for connecting links is presented in Fig. 5. Although only a few data points are available, a correlation similar to that for the major components is effected. In this case, however, the numbers at each data point correspond to the frequency of a given mode of the connecting link apparatus. The types of modes were also qualitatively identified, but no correspondence with the analytical model was possible because of the type of model postulated. Therefore, these mode shapes will not be discussed.

It can be seen that one test was performed also on a single flexure, and was found to fall near the same correlation line when the energy data were doubled to allow for two springs. Even so, some scatter in the data does occur. At this point it must be admitted that these are the weakest results of the entire study, and will carry into some errors in damping predictions for the lower modes later.

Finally, it can be noted that only a single point is present for the 3-D pin joint, since only one vertical mode could be excited with the procedure utilized. This point fell within the scatter of the correlation line for the flexure joints. As a result, at first we considered using the same correlation line for the damping of vertical motion of the 3-D pins. However, upon further reflection, we used the indicated 45° correlation

Table 1 Component frequencies and damping for free-free suspension

Mode Identification	Theoretical Frequency Hz	Experimental Frequency Hz	Experimental Damping Ratio
a. H/O tank			
1SBF	69.4	68.4	0.00394
1VBF	77.0	79.8	0.00276
1LQF	96.7	95.0	0.00718
2SBF	150	169	0.00370
2VBF	165	159	0.00362
2LQF	170	186	0.00680
1TF	207	...	...
3LQF	232	238	0.01100
3SBF	257	274	0.00462
3VBF	261	264	0.00466
4VBF	320	...	...
2TF	324	...	...
4SBF	393	435	0.00525
4LSF	394	365	0.00276
b. Orbiter			
1BF	150	148	0.0142
1TF	193	192	0.0153
1LF	377	386	0.0162
2BF	396	394	0.0168
2TF	494	...	...
3BF	642	646	0.0172
4BF	703	739	0.0200
3TF	801	...	...
2LF	967	897	0.0179
c. Port SRM			
1BF	50.8	50.0	0.0110
2BF	161	163	0.0136
1TF	211	203	0.0154
3BF	287	298	0.0158
2TF	349	...	...
1LF	351	350	0.0166
4BF	405	432	0.0182
2LF	588	584	0.0190
5BF	597	...	...
d. Starboard SRM			
1BF	50.8	50.6	0.0112
2BF	161	164	0.0145
1TF	211	205	0.0162
3BF	287	296	0.0163
2TF	349	...	...
1LF	351	355	0.0170
4BF	405	437	0.0186
2LF	588	595	0.0187
5BF	597	...	...

Note: VB = vertical bending; SB = side bending; LQ = longitudinal liquid; LS = longitudinal structure; and T = torsion.

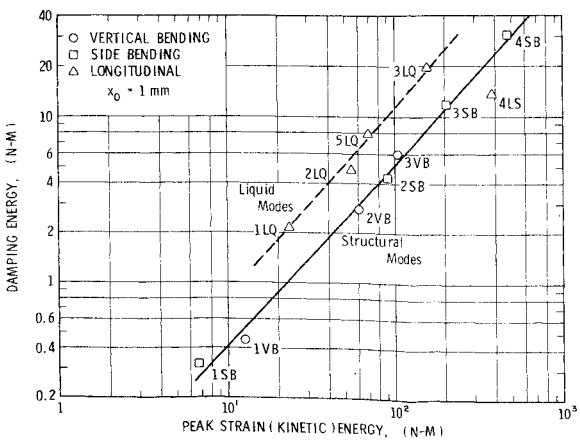

Fig. 3 Experimental damping energy for H/O tank.

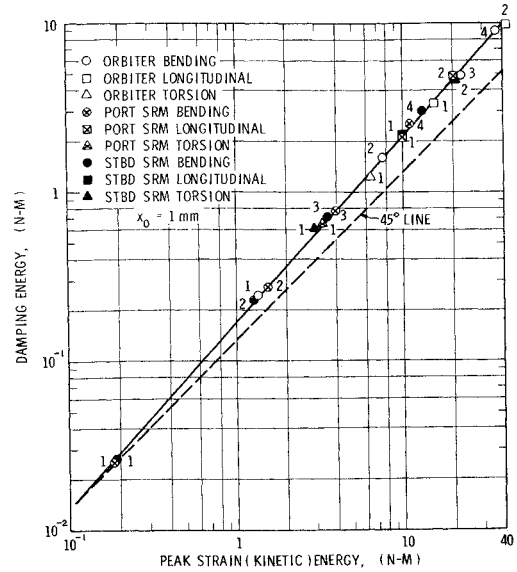

Fig. 4 Experimental damping energy for orbiter and solid rocket motors.

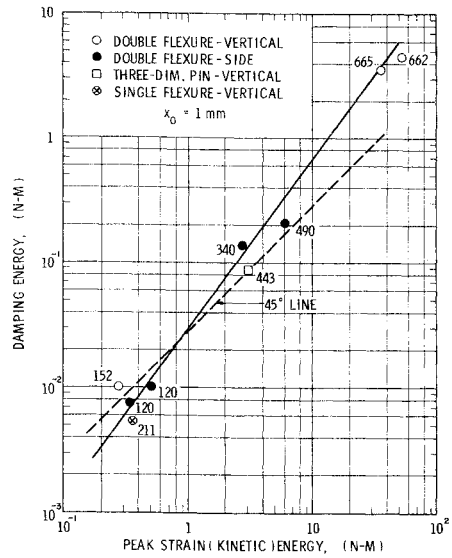

Fig. 5 Experimental damping energy for connecting links.

line, since such a line represents constant specific damping (damping ratio) in the range where no other modes were present. Damping for motion in lateral and longitudinal directions was neglected at the pivot. Again, it is admitted that a more detailed investigation of the joints would have been appropriate, and in fact, was attempted. However, no further useful information was obtained during the time available.

Method of Damping Prediction

The basic energy method of damping prediction used for this study is essentially the same as that formulated in detail in Ref. 2. However, in this case one modification is necessary. In order to be realistic, no damping forces relative to ground are included in the model. As a result, purely rigid body motion of the components relative to the spring supports contribute no damping energy to the system modes (the spring supports themselves do, of course), but do contribute to kinetic energy of the system modes. Thus, it is postulated that only component elastic, or strain energy, is the appropriate parameter to consider for the present application, rather than modal kinetic energy. For freely supported component testing, these two parameters are equal, as has been noted in Figs. 3-5.

We now will indicate how these curves are used to predict damping for system modes, as summarized in Fig. 6. We start

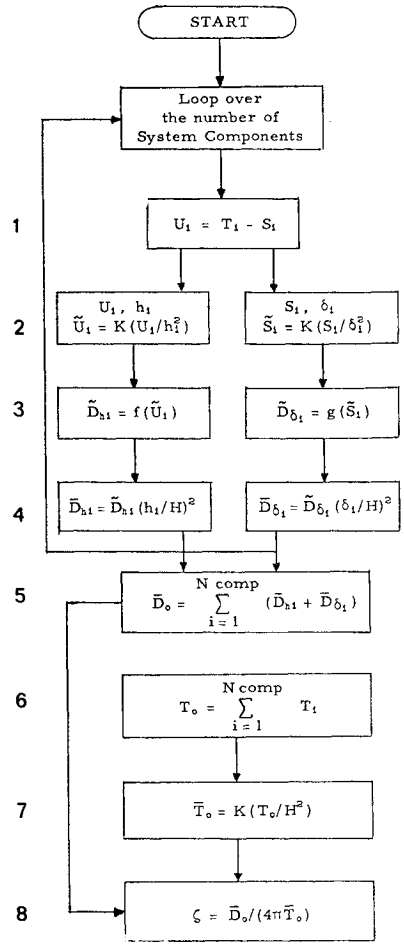

Fig. 6 Flow diagram for damping calculations. 1) Determine strain energy U_i from spring support strain energy S_i and component kinetic energy T_i. 2) Compute strain energy relative to 1.0 mm maximum deflection. K ~ constant for proper units. 3) Determine damping energy from free-free experimental curves, Figs. 3-5. 4) Compute damping energy relative to 1.0 mm maximum coupled system deflection H. 5) Compute total system damping energy. N comp ~ number of system components. 6) Compute system total kinetic energy. 7) Compute system total kinetic energy relative to 1.0 mm maximum coupled system deflection H. 8) Compute modal damping.

with the results from the free vibration eigenvalue problem, which provides system natural frequencies, and corresponding system eigenvectors for all components and connecting links of the system. Within each system eigenvector, of maximum amplitude H, each component experiences a maximum amplitude h_i and each spring support experiences a maximum deflection δ_i, whose values are determined by the system of units used for the analysis.

Step 1: Calculate kinetic energy T_i for each component at amplitude h_i by means of the component eigenvectors and modal mass matrices. Calculate strain energy S_i at amplitude δ_i for all connecting links associated with the ith component by means of the component eigenvectors and link stiffness matrices. We then can calculate component strain energy at amplitude h_i from $U_i = T_i - S_i$. For those components where the connecting links are not part of the component, $U_i = T_i$. Thus, Step 1 can be eliminated if the connecting links are modeled as separate components themselves.

Step 2: The empirical data of Figs. 3, 4, and 5 are in terms of strain energies expressed in metric units, and normalized to $X_0 = 1$ mm maximum amplitude. Therefore, we must convert the above energies by means of

$$\tilde{U}_i = K(U_i/h_i^2)$$
$$\tilde{S}_i = K(S_i/\delta_i^2) \qquad X_o = 1 \text{ mm}$$

where K is a constant that provides metric units.

Step 3: The energies of Step 2 are now used to enter the respective curves of Figs. 3-5. Damping energies $\tilde{D}_{hi}$ and $\tilde{D}_{\delta i}$, each at $X_0 = 1$ mm deflection are obtained from the curves of the form

$$\tilde{D}_{hi} = f(\tilde{U}_i)$$
$$\tilde{D}_{\delta i} = g(\tilde{S}_i) \qquad X_o = 1 \text{ mm}$$

Setp 4: We now adjust the damping energy levels to the proper component and spring amplitudes that occur in a given system mode of maximum amplitude $H = 1$ mm. This is done by the equations

$$\bar{D}_{hi} = \tilde{D}_{hi}(h_i/H)^2$$
$$\bar{D}_{\delta i} = \tilde{D}_{\delta i}(\delta_i/H)^2 \qquad H = 1 \text{ mm}$$

Step 5: Compute the total system damping energy $\bar{D}_o$ for a given mode by summing over all the components and their spring supports:

$$\bar{D}_o = \sum_{i=1}^{N\,\text{comp}} (\bar{D}_{hi} + \bar{D}_{\delta i})$$

Step 6: Compute system total kinetic energy by summing over the kinetic energies of all components:

$$T_o = \sum_{i=1}^{N\,\text{comp}} T_i$$

Step 7: Adjust system kinetic energy to $H = 1$ mm maximum modal deflection and convert to metric units.

$$\bar{T}_o = K(T_o/H^2)$$

Step 8: Compute damping ratio for a given system mode from

$$\zeta = \bar{D}_o/(4\pi\bar{T}_o)$$

It must be emphasized that the above procedure includes the assumption of linearity of damping *forces* with amplitude. However, it also allows for a nonlinear relationship between damping energy and strain energy, as is apparent from Figs. 3-5.

Combined System Results

Theoretical results for all modes within a 400-Hz frequency range are presented in Tables 2a and 2b. The identification of the modes refers back to the basic modal identification presented in Fig. 2a for the free-free configurations. Of course, because of coupling, the exact shape of the combined modes is different in many cases.

Since the data represents modes of a relatively complex three-dimensional structure, rather than try to depict mode shapes in some type of isometric view, it was decided to describe the modes in terms of the fractional part of the total kinetic energy that was presented in each type of motion in each component. In this regard, it must be emphasized that vertical and side motion of the SRMs are designated relative to their respective mounting springs, and neither of these axes are parallel to the vertical and side axes of the orbiter and H/O tank. Also, the modes are designated as symmetric and antisymmetric relative to a plane which passes through the centerlines of the orbiter and H/O tank.

The real meat of this entire study is now presented in Table 3 for the modes which have just been described. Frequency and damping comparisons are presented. Frequency results are seen to be remarkable for so wide a range and number and variety of modes present. Damping results overall are in good agreement, but need considerable discussion. Predicted damping values are given for those which include energy dissipated within the major components (structures) alone, and also for the total which includes that predicted to be dissipated within the connecting links. Of course, the total figure is that which must be compared with the measured

Table 2 Theoretical frequencies and kinetic energy distribution

Mode Identification	Theoretical Frequency HZ	H/O Longitudinal Motion	H/O Vertical Motion	ORB Vertical Motion	SRM Vertical[a] Motion	SRM Side[a] Motion
a. Symmetric Modes						
Roll/SRM	13.9	0	0.109	0.010	0.002	0.879
Pitch/SRM	25.7	0.042	0	0.229	0.726	0.003
Roll/SRM	28.9	0.034	0.026	0.312	0.107	0.521
Roll/SRM& Pitch/ORB	30.1	0.028	0.153	0.299	0.199	0.321
Pitch/SRM	35.3	0.222	0.004	0.070	0.703	0.001
Pitch/ORB	47.4	0.003	0.052	0.914	0.016	0.015
1VB/SRM	52.8	0	0.013	0.012	0.973	0.002
1SB/SRM	60.0	0	0.151	0.021	0.002	0.826
1VB/HO	75.7	0	0.604	0.166	0.011	0.219
1LQ/HO	97.2	0.998	0	0.002	0	0
1T/SRM	103.0	0	0.049	0.126	0.001	0.824
2VB/SRM	123.0	0	0.045	0.056	0.899	0
1VB/ORB	132.0	0	0.326	0.564	0.081	0.029
2VB/HO	162.0	0.012	0.463	0.307	0.027	0.191
2SB/SRM	164.0	0.007	0.062	0.119	0.004	0.808
2LQ/HO	171.0	0.967	0.008	0.006	0.018	0.001
2VB/SRM	175.0	0.014	0.019	0.017	0.950	0
VB/HO-ORB	190.0	0	0.462	0.496	0.003	0.039
3LQ/HO	233.0	1.000	0	0	0	0
3VB/HO	262.0	0	0.937	0.002	0.001	0.060
3SB/SRM	275.0	0	0.066	0.001	0	0.933
4VB/SRM	293.0	0	0.002	0	0.998	0
4SB/SRM	310.0	0	0.112	0	0	0.888
4VB/HO	322.0	0	0.918	0.001	0.001	0.080
1L/SRM	337.0	0	0	0	1.000	0
2T/SRM	353.0	0	0.005	0	0	0.995
1L/ORB	379.0	0.002	0	0.998	0	0
4LS/HO	394.0	0.951	0	0.049	0	0
3VB/ORB	399.0	0.048	0.001	0.951	0	0
5VB/SRM	411.0	0	0	0	1.000	0
b. Antisymmetric Modes						
Roll/ORB-SRM	14.7	0.011	0.029	0.582	0.014	0.364
Yaw/SRM	25.3	0.209	0.003	0.132	0.038	0.618
Pitch/SRM	26.9	0.044	0.162	0.025	0.748	0.021
Yaw/SRM	29.4	0.248	0.026	0.093	0.023	0.610
Pitch/SRM	31.7	0	0.051	0.001	0.946	0.002
Yaw/ORB	47.5	0.003	0.131	0.835	0.024	0.007
1VB/SRM	54.7	0.001	0.168	0.013	0.818	0
1SB/SRM	61.6	0.002	0.004	0.010	0.003	0.981
1SB/HO	75.7	0.001	0.724	0.078	0.175	0.022
IT/SRM	103.0	0.043	0.015	0.346	0.010	0.586
1SB/ORB	117.0	0.191	0.143	0.464	0.028	0.174
2VB/SRM	123.0	0.030	0.278	0.064	0.597	0.031
2SB/ORB	155.0	0.003	0.208	0.636	0.152	0
2B/HO-ORB-SRM	162.0	0.012	0.293	0.346	0.302	0.047
2SB/SRM	163.0	0.014	0.013	0.014	0.014	0.945
3VB/SRM	183.0	0.002	0.315	0.019	0.664	0
1T/HO	213.0	0.748	0.004	0.061	0	0.187
1T/ORB	234.0	0.076	0.031	0.886	0	0.007
3SB/HO	259.0	0.001	0.982	0.007	0.006	0.004
3SB/SRM	277.0	0.065	0.004	0	0	0.931
4VB/SRM	291.0	0.001	0.210	0.001	0.788	0
SB/HO	301.0	0.009	0.767	0.005	0.219	0
4SB/SRM	310.0	0.296	0.005	0.005	0	0.694
1L/SRM	337.0	0.001	0	0	0.999	0
2T/HO	338.0	0.682	0.006	0.009	0.001	0.302
2T/SRM	355.0	0.086	0.001	0.001	0	0.912
4SB/HO	394.0	0	0.996	0.003	0.001	0
3SB/ORB	396.0	0	0.003	0.997	0	0
5VB/SRM	411.0	0	0.004	0	0.996	0

[a] Both port and starboard SRM included.

values, although joint dissipation affects the lower modes principally.

In general, it can be seen that significant discrepancies in damping exist for some of the lower modes where connecting link damping is dominant. This reflects that a good modeling and, for that matter, damping energy correlation (Fig. 5) has not been achieved. However, except for a few isolated cases, better agreement has been achieved for those modes where major component structural response, rather than connecting link response is dominant. Thus, a good damping correlation (Figs. 3 and 4) has been achieved in this regard, and the damping prediction method has been validated within reasonable limits.

The few isolated discrepancies that can be found at the higher frequencies were found to be result of some anomaly in the modal response. In some cases, a mixing of symmetric and

Table 3 System frequencies and damping

A. Symmetric Modes

Mode Identification	Theoretical Frequency Hz	Experimental Frequency Hz	Predicted Damping Ratio (Structure)	Predicted Damping Ratio (Total)	Experimental Damping Ratio	Damping Error Percent
Roll/SRM	13.9	14.6	0.00025	0.00074	0.00179	310
Pitch/SRM	25.7	28.9	0.00288	0.00324	0.00420[d]	(23)
					0.00651	(50)
Roll/SRM	28.9	...	0.00310	0.00329	...	
Roll/SRM & Pitch/ORB	30.1	...	0.00298	0.00324	...	
Pitch/ORB	35.3	38.2	0.00104	0.00128	0.00353	64
Pitch/ORB	47.4	46.4	0.00014	0.00128	0.00081	58
1VB/SRM	52.8	55.8	0.002600	0.003560	0.00365[b]	2
1SB/SRM	60.0	63.0	0.00667	0.00670	0.00720	7
1VB/HO	75.7	81.7	0.00324	0.00349	0.00327	7
1LQ/HO	97.2	96.7	0.00703	0.00703	0.00500[d]	(40)
					0.00650	(8)
1T/SRM	103.0	116.0	0.00580	0.00679	0.00539[d]	(26)
					0.00660	(3)
2VB/SRM	123.0	130.0	0.00429	0.00696	0.00779[d]	(11)
					0.01100	(37)
1VB/ORB	132.0	135.0	0.00449	0.00570	*b*	
2VB/HO	162.0	160.0	0.00746	0.00760	0.00420[d]	(81)
					0.00646	(18)
2SB/SRM	164.0	165/170[a]	0.01208	0.01208	0.00561	115
2LQ/HO	171.0	187.0	0.00661	0.00661	0.00399[d]	(66)
					0.00595	(11)
3VB/SRM	175.0	188.0	0.00872	0.00970	0.00616[d]	(57)
					0.00770	(26)
VB/HO-ORB	190.0	198.0	0.00159	0.00368	0.00489	(25)
					0.00604	(39)
3LQ/HO	233.0	237.0	0.00802	0.00802	...	
3VB/HO	262.0	267.0	0.00418	0.00418	0.00325[d]	(29)
					0.00417	(0)
3SB/SRM	275.0	283.0	0.01240	0.01240	*b*	
4VB/SRM	293.0	305.0	0.01340	0.01340	0.01560	14
4SB/SRM	310.0	305.0	0.00942	0.01060	0.01110	5
4VB/HO	322.0	...	0.00427	0.00422	...	
1L/SRM	337.0	349.0	0.01610	0.01610	0.01610	0
2T/SRM	353.0	357.0	0.01530	0.01530	0.16100[b]	5
1L/ORB	379.0	388.0	0.01600	0.01600	0.16300[b]	2
4LS/HO	394.0	366.0	0.009660	0.00966	0.00177[d]	(445)
					0.00329	(194)
3VB/ORB	399.0	400.0	0.01630	0.1630	0.01740	6
5VB/SRM	411.0	431.0	0.01540	0.01540	*b*	

B. Antisymmetric Modes

Roll/ORB-SRM	14.7	15.3	0.00101	0.00163	0.00101	61
YAW/SRM	25.3	...	0.00321	0.00349	...	
Pitch/SRM	26.9	25.6	0.00079	0.00105	...	
YAW/SRM	29.4	32.1[a]	0.00056	0.00145	0.00135[d]	(7)
					0.00197	(26)
Pitch/SRM	31.7	30.8[a]	0.00384	0.00424	0.00335	27
YAW/ORB	47.5	50.2	0.00640	0.00640	0.00277	131
1VB/SRM	54.7	53.6	0.00325	0.00394	0.00308	28
1SB/SRM	61.6	65.1	0.00676	0.00676	0.00712	5
1SB/HO	75.7	74.2	0.00209	0.00233	0.00349	33
1T/SRM	103.0	116.0	0.00490	0.00595	0.00539[d]	(10)
					0.00660	(10)
1SB/ORB	117.0	108.0	0.00335	0.00449	0.00488	8
2VB/SRM	123.0	130.0	0.00362	0.00537	0.00779[d]	(31)
					0.01100	(51)
2SB/ORB	155.0	...	0.01030	0.01040	...	
2B/HO-ORB-SRM	162.0	169.0	0.00797	0.00811	*b*	
2SB/SRM	163.0	...	0.01200	0.01200	...	
3VB/SRM	183.0	180.0	0.00452	0.00610	0.00710[b]	14
IT/HO	213.0	...	0.00456	0.00456	...	
1T/ORB	234.0	230.0	0.00810	0.00910	0.00840[b]	8
3SB/HO	259.0	261.0	0.00373	0.00373	0.00333	12
3SB/SRM	277.0	...	0.01250	0.01250	*b*	
4VB/SRM	291.0	305.0[c]	0.01200	0.01200	0.01560	23
SB/HO	301.0	...	0.00614	0.00614	...	
4SB/SRM	310.0	305.0[c]	0.01140	0.01140	0.01110	3
1L/SRM	337.0	349.0	0.01620	0.01620	0.01610	0
2T/HO	338.0	326.0	0.00673	0.00673	*b*	
2T/SRM	355.0	357.0	0.01530	0.01530	0.0161[b]	5
4SB/HO	394.0	...	0.00384	0.00384	...	
3SB/ORB	396.0	399.0	0.01710	0.01710	0.01650	4
5VB/SRM	411.0	431.0	0.01540	0.01540	*b*	

Note: [a] mixed modes; [b] beating; [c] influenced by exciter location; [d] double values indicate nonlinearity range.

nonsymmetric modes occurred, and in others a distortion in mode shape from that predicted theoretically. Likewise, in some cases data could not be obtained because of beating between modes, or a loss of a weak mode within a nearby more dominant mode. The sources of damping nonlinearity with amplitude were not identified, although were noted to exist for some modes. Finally, some errors may have been caused by the postulation of identical prediction models for the SRMs. One might expect that some differences in both frequencies and damping occurred for the models, since exact identity is never possible physically. This probably was a major cause of beating nonlinearities, and mixing of modes in the combined system.

In view of the previous comments, a final conclusion is in order with regard to the types of damping energy correlations that can be expected from built-up construction that will be present in prototype Shuttle components. It appears from Fig. 4 that single-line correlation for all kinds of modes occurs only for a component whose strain energy is absorbed within a structure of uniform or homogeneous material. Such a case is the exception, rather than the rule in typical aerospace construction. Thus, it may occur that individual correlation lines will be found for each type of mode (i.e., bending, longitudinal structure, longitudinal liquid, propellant slosh, etc.). This result is still completely amenable to the energy approach to damping prediction in the combined system, so long as the energy components of the coupled modes are properly identified.

References

[1]Proceedings of Symposium on Substructure Testing and Synthesis, NASA Space Shuttle Dynamics and Aeroelasticity Working Group Meeting, Marshall Space Flight Center, Aug. 1972.

[2]Kana, D.D. and Huzar, S., "Synthesis of Shuttle Vehicle Damping Using Substructure Test Results," *Journal of Spacecraft and Rockets*, Vol. 10, Dec. 1973, pp. 790-797.

[3]Kana, D.D. and Unruh, J.F., "Prediction of Shuttle Vehicle Damping From Component Test Results," Final Rept., Contract NAS8-27569, March 1973, Southwest Research Institute, San Antonio, Texas.

[4]Kana, D.D. and Nagy, A., "An Experimental Determination of the Longitudinal Modes of a Simulated Launch Vehicle Dynamic Model," Interim Report, Contract NAS8-30167, March 1970, Southwest Research Institute, San Antonio, Texas.